

## Catalytic oxidation of ethyl acetate by copper modified Ce-Mn and Ce-Ti mesoporous nanostructured oxides

R. N. Ivanova<sup>1\*</sup>, M. D. Dimitrov<sup>1</sup>, G. S. Issa<sup>1</sup>, D. G. Kovacheva<sup>2</sup>, T. S. Tsoncheva<sup>1</sup>

<sup>1</sup> Institute of Organic Chemistry with Centre of Phytochemistry, BAS, Bulgaria

<sup>2</sup> Institute of General and Inorganic Chemistry, BAS, Sofia, Bulgaria

Received October 28, 2018; Accepted December 11, 2018

Ceria-based materials continue to be investigated for their structural and chemical reduction behaviour and non-stoichiometry, oxygen storage capacity and metal-ceria interactions. These materials show promising application as catalysts for environmental protection. In the current investigation mesoporous ceria-titania and ceria-manganese binary oxides were used as a host matrix of nanosized copper oxide species. The textural, structural and redox properties of the obtained composites were investigated using Nitrogen physisorption, X-ray diffraction, UV-Vis, Raman spectroscopy as well as temperature-programmed reduction with hydrogen. Their catalytic activity for total oxidation of volatile organic pollutants was studied using ethyl acetate as a probe molecule. The state of the loaded copper species and the related catalytic behavior depends on the degree of defectness of the metal oxide support, which could be controlled by using binary oxide systems.

**Keywords:** mesoporous nanostructured ceria-titania, ceria-manganese oxides, total oxidation of ethyl acetate, copper oxide.

### INTRODUCTION

Metal oxides represent one of the most important and widely employed categories of solid catalysts, either as active phases or as supports. Metal oxides are utilized both for their acid–base and redox properties and constitute the largest family of catalysts in heterogeneous catalysis. Transition and noble group metals are frequently used as catalyst components and their activity has been attributed to the outer electron configuration [1]. Among the metal oxide catalysts, those of transition metals occupy a predominant place owing to their low cost of production, easy regeneration and selective reactivity. They are used in widely different types of organic reactions, such as oxidation, dehydration, dehydrogenation and isomerization [2]. Their catalytic activity may be traced to the presence of partially filled d-shells of the metal ion and to the influence of the oxide ligand field on this partially filled d-shell. Among the transition metal and rare earth mixed oxide catalysts, the  $\text{MnO}_x\text{-CeO}_2$  mixed

oxides have been found to be promising catalysts that can be practically used for some oxidation reactions. For the synergistic mechanism between  $\text{MnO}_2$  and  $\text{CeO}_2$ , the binary oxides exhibited good catalytic activity for the oxidation of ammonia in supercritical water [3]. Moreover, the  $\text{MnO}_x\text{-CeO}_2$  catalysts also showed high activity for complete oxidation of formaldehyde and methane at low temperature due to more  $\text{Mn}^{4+}$  ions and richer lattice oxygen [4, 5]. Previous investigations have shown that the catalytic activity is strongly influenced by the composition of  $\text{MnO}_x\text{-CeO}_2$  mixed oxide catalysts [6]. It has been well accepted that the interactions between  $\text{MnO}_x$  and  $\text{CeO}_2$  vary with composition, resulting in the evolution of their textural, structural, and oxidation state [6, 7]. On the other hand, titanium oxide has received much attention in many technological areas. Doping titania with transition metals (Ce, Mn, Zr, Sn, Cu, etc.) can increase its catalytic activity and thermal stability as a result of specific interaction between the various metal oxide particles [8, 9]. It was established that the activity and selectivity of copper containing catalysts depend to great extent on the dispersion of the  $\text{CuO}_x$  species which could be regulated by the surface and texture properties of the support [10–12]. Besides, it is known that copper–cerium materials could be considered as effective oxidation catalysts, though

\* To whom all correspondence should be sent:  
E-mail: radostinaiv@abv.bg

their performance in volatile organic compounds (VOCs) oxidation is scarcely studied, however, our previous investigations have shown that the stabilization of highly dispersed copper oxide particles over the ceria surface improves the catalytic activity in ethyl acetate total oxidation [13].

The aim of current investigation is to study the effect of mesoporous ceria-titania and ceria-manganese binary oxides on the state of the supported on them copper oxide nanoparticles. The structural, redox and catalytic properties of the obtained composites were characterized by Nitrogen physisorption, X-ray diffraction, UV-Vis and Raman spectroscopy as well as temperature-programmed reduction with hydrogen. The effect of copper modification on the catalytic behavior of mesoporous ceria-manganese and ceria-titania binary oxides was studied in total oxidation of ethyl acetate as a member of volatile organic compounds (VOCs).

## EXPERIMENTAL

### *Materials*

Mono- and bi-component ceria-manganese and ceria-titania oxide supports were synthesized by template-assisted technique using N-cetyl-N,N,N-trimethyl ammonium bromide (CTAB) as a template and hydrothermal treatment at 373 K. For the purpose, 12.0 g CTAB were dissolved in 100 ml distilled water and then slowly and under vigorous stirring a second solution containing 0.02918 moles total of metal chlorides ( $\text{TiCl}_4$ ,  $\text{CeCl}_3 \cdot 7\text{H}_2\text{O}$ ,  $\text{MnCl}_2 \cdot 4\text{H}_2\text{O}$ ) dissolved in 50 ml distilled water and in proportion of 5:5 mol ratio for the bi-component materials were added. Then, the temperature was raised to 323 K and the reaction mixture was stirred for 30 min before adding of 20 ml  $\text{NH}_3$  (25%). The resulting mixture was stirred overnight at 323 K, then transferred into an autoclave and treated at 373 K for 24 h. The obtained samples were filtrated, washed with distilled water, dried at room temperature and calcined up to 773 K with a ramp of 1 K/min and dwelling time of 10 h at the final temperature. Copper oxide was supported by incipient wetness impregnation (WI) of the obtained mono- and bi-component metal oxide supports with 0.5 ml aqueous solution of  $\text{Cu}(\text{NO}_3)_2 \cdot 3\text{H}_2\text{O}$  in amount necessary for the loading of 8 wt.% of copper, followed by drying in ambient atmosphere overnight and its further decomposition in air at 773 K for 2 hours.

### *Methods of characterization*

Powder X-ray diffraction patterns were collected on Bruker D8 Advance diffractometer equipped

with Cu K $\alpha$  radiation and LynxEye detector. Nitrogen sorption measurements were recorded on a Quantachrome NOVA 1200e instrument and a Beckman Coulter SA 3100 apparatus at 77 K. Before the physisorption measurements the samples were out gassed at 423 K overnight under vacuum. The UV-Vis spectra were recorded on a Jasco V-650 UV-Vis spectrophotometer equipped with a diffuse reflectance unit. Raman spectra were acquired with a DXR Raman microscope (Thermo Fischer Scientific, Inc., Waltham, MA) using a 780 nm laser. The TPR/TG (temperature-programmed reduction/thermogravimetric) analyses were performed in a Setaram TG92 instrument. Typically, 40 mg of the sample were placed in a microbalance crucible and heated in a flow of 50 vol.%  $\text{H}_2$  in Ar ( $100 \text{ cm}^3 \text{ min}^{-1}$ ) up to 773 K at  $5 \text{ K min}^{-1}$  and a final hold-up of 1 h. The catalytic oxidation of ethyl acetate was performed in a flow type reactor (0.030 g of catalyst) with a mixture of ethyl acetate in air (1.21 mol%) and WHSV of 100 h $^{-1}$ . Before the catalytic experiments the samples were treated in argon at 373 K for 1 h. The experimental data were obtained under temperature-programmed regime in the range of 473–773 K. Gas chromatographic analyses were done on a HP 5890 apparatus using carbon-based calibration. The products distribution was calculated as  $\text{CO}_2$  ( $S_{\text{CO}_2}$ ), acetaldehyde ( $S_{\text{AA}}$ ), ethanol ( $S_{\text{Et}}$ ) and acetic acid ( $S_{\text{AcAc}}$ ) selectivity by the equation:  $S_i = Y_i/X \cdot 100$ , where  $S_i$  and  $Y_i$  were the selectivity and the yield of (i) product and X was the conversion. For more precise comparison, the conversion was normalized to unit surface area ( $SA = X/A$ , where X was the conversion at 650 K and A was the specific surface area of the corresponding sample).

## RESULTS AND DISCUSSION

### *Structural characterization*

Some physicochemical characteristics of the obtained samples are presented in Table 1. For comparison data for the corresponding supports are also given. Nitrogen physisorption measurements were conducted in order to elucidate the textural properties of the studied samples. All obtained materials exhibit relatively high specific surface area and pore volume. Note, that the modification with copper leads to significant decrease in the texture features, probably as a result of pore blocking due to copper deposition within the pores of the support.

X-ray diffraction technique (XRD) has been used for determination of samples crystallinity and phase composition (Fig. 1, Table 1). Pure ceria as well as all cerium-containing samples show well

**Table 1.** Nitrogen physisorption and XRD data of pure supports and copper modified materials

Sample	Space Group	Unit cell, Å	Particles size, nm	BET, m <sup>2</sup> /g	Total Pore Volume, ml/g
TiO <sub>2</sub>	Anatase, syn	3.786	17.4	85	0.29
	Tetragonal – Body-centered I41/amd	9.493			
Cu/TiO <sub>2</sub>	Anatase, syn	3.786	20.8	40	0.24
	Tetragonal – Body-centered I41/amd	9.488			
	Tenorite	4.691	36.4		
		3.419			
5.138					
99.594					
Ce-Ti	Cerium oxide	5.403	12.0	99	0.45
	Cubic – Face center – Fm-3m				
Cu/CeTi	Cerium oxide	5.405	12.5	69	0.39
	Cubic – Face center – Fm-3m				
	Tenorite	4.716	45.8		
		3.431			
5.126					
99.578					
Mn <sub>x</sub> O <sub>y</sub>	24% Mn <sub>2</sub> O <sub>3</sub> (Ia-3)		85	7.4	0.025
	67% Mn <sub>5</sub> O <sub>8</sub> (C2/m)		33		
	9% Mn <sub>3</sub> O <sub>4</sub> (I41/amd)		66		
Cu/Mn <sub>x</sub> O <sub>y</sub>	Mn <sub>2</sub> O <sub>3</sub> Bixbyte C (Ia-3) (71-636)	9.412	62	5.7	0.02
	Mn <sub>5</sub> O <sub>8</sub> (C2/m) (72-1427)	10.377	24		
		5.726			
		4.871			
		109.39			
	CuO (C2/c)	4.774	60		
		3.330			
		5.126			
99.93					
CuMn <sub>2</sub> O <sub>4</sub> (Fd-3m)	8.288	32			
Ce-Mn	84% CeO <sub>2</sub> (Fm-3m)	5.334	7	65.6	0.47
	12% Mn <sub>5</sub> O <sub>8</sub> (C2/m)				
	4% Mn <sub>2</sub> O <sub>3</sub> (Ia-3)				
Cu/CeMn	Fm-3m	5.35	7	58.3	0.40
	Mn <sub>5</sub> O <sub>8</sub> C2/m (72-1427)	10.31	13		
		5.68			
		4.89			
		108.9			
	CuO (C2/c) – traces	4.8	6		
3.36					
5.3					
99					
CeO <sub>2</sub>	Cerium oxide	5.413	21.8	46	0.26
	Cubic – Face center – Fm-3m				
Cu/CeO <sub>2</sub>	Cerium oxide	5.413	22.0	24	0.20
	Cubic – Face center – Fm-3m				
	Tenorite	4.679	29.3		
		3.440			
5.130					
99.44					

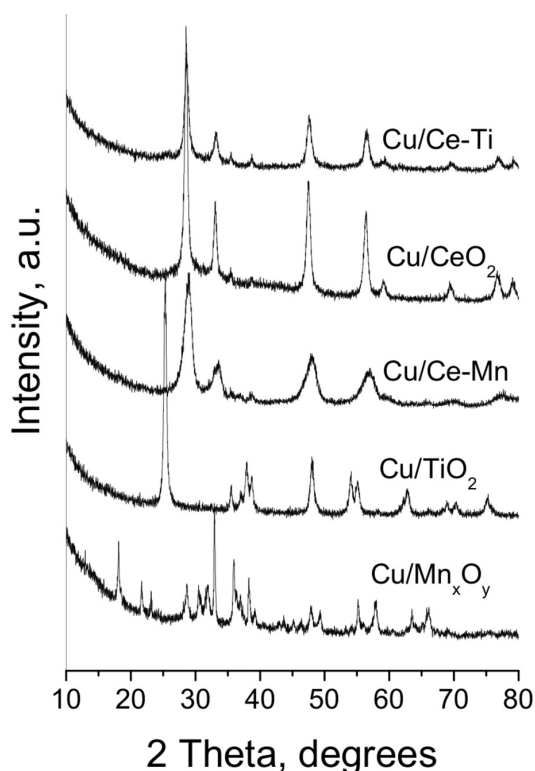


Fig. 1. XRD patterns of all studied materials.

defined reflections of cubic fluorite-like structure with variations in particle sizes. It should be noted that the unit cell parameter is smaller for the mixed oxide samples, which could be an indication of partial Ti, Mn or Cu introduction within the ceria fluorite structure. Anatase phase with average crystallite sizes of about 17 nm is registered for pure  $\text{TiO}_2$ . No significant changes in the lattice parameters for titania occur after the modification with copper. The XRD patterns of copper modified materials contain reflections at  $2\theta = 35.5^\circ$ ,  $38.5^\circ$  and  $48.5^\circ$ , which are due to the presence of well crystallized tenorite phase (space group  $C2/c$ , ICDDPDF2#48-1548). The observed relatively large CuO crystallite size indicates their partial location on the outer surface of the mesoporous oxide support (Fig. 1, Table 1). The absence of any additional reflections of copper oxide phase for Cu/CeMn sample could be due the fine dispersion of the supported phase, but we cannot fully exclude also better mixing of the oxides and the obtaining of a structure with high degree of defectiveness. This is well demonstrated by the changes in the unit cell parameters of the corresponding phases (Table 1). For Cu/Mn<sub>x</sub>O<sub>y</sub> sample, presence of CuMn<sub>2</sub>O<sub>4</sub> phase is registered as well, which suggests strong interaction between the copper species and the support.

### Spectral measurements

Raman spectroscopy was applied for better understanding the microstructure of the obtained materials (Fig. 2a). The Raman shifts in the spectrum of Cu/TiO<sub>2</sub> confirm the XRD analyses for the presence of pure anatase phase (peaks at about  $143\text{ cm}^{-1}$  (E1g),  $195\text{ cm}^{-1}$  (E2g),  $396\text{ cm}^{-1}$  (B1g),  $514\text{ cm}^{-1}$  (A1g) and  $637\text{ cm}^{-1}$  (E3g)). The additional bands at about  $297$ ,  $344$ ,  $629\text{ cm}^{-1}$  correspond to well crystalline CuO phase [14]. The spectrum of Cu/CeO<sub>2</sub> show the main Raman shift at  $463\text{ cm}^{-1}$  (E2g) typical of CeO<sub>2</sub>. The appearance of additional band at  $600\text{ cm}^{-1}$  indicates presence of oxygen vacancies in the ceria lattice probably originated with the interaction between CeO<sub>2</sub> and CuO. Such interaction between the copper species and Mn<sub>x</sub>O<sub>y</sub> support is considered on the base of the observed weak and less intensive CuO bands for the Cu/Mn<sub>x</sub>O<sub>y</sub> sample, which is consistent with the XRD results. Significant variations in the dispersion of the loaded copper particles occur when binary oxides were used as a support (Fig. 2a). For the Cu/Ce-Ti sample, well resolved Raman shifts, typical of relatively large CuO crystallites, are observed which is in consistence with the XRD data. Just the opposite, the observed very low intensive Raman shifts in the spectrum of Cu/Ce-Mn indicate improved dispersion for all metal oxides in the composite, which could be due to the existence of strong interaction between them.

UV-Vis analyses were performed in order to get information about the absorption properties of the obtained materials (Fig. 2b). The strong absorption feature in the UV-Vis spectrum of titania modification above 350 nm is due to d-d electronic transition between  $\text{Ti}^{4+}$ -ion and  $\text{O}^{2-}$  ligand in pure anatase [15], which is consistent with the XRD data. The spectrum of ceria modification displays absorption in the 300–500 nm range corresponding to  $\text{Ce}^{4+} \leftarrow \text{O}^{2-}$  charge transfer, which is typical of ceria phase [16]. Formation of oxygen vacancies and high amount of  $\text{Ce}^{3+}$  could also be suggested. The spectrum of manganese oxide modification represents absorption feature, which is due to variations in manganese oxidation state ( $\text{Mn}^{2+}$ ,  $\text{Mn}^{3+}$ , and  $\text{Mn}^{4+}$ ) [17]. The observed continuous absorption in the 400–800 nm region for this sample reveals changes in the environment of Mn and Cu ions, which is consistent with the assumption of the XRD data (Fig. 1, Table 1) for the formation of CuMn<sub>2</sub>O<sub>4</sub> mixed oxide phase. The absorption in the range of 240–320 nm and 600–800 nm regions for all copper modification is related to  $\text{O}^{2-} \rightarrow \text{Cu}^{2+}$  CT and d-d transitions, respectively, of crystalline CuO [18]. They are most pronounced for the CeO<sub>2</sub>-TiO<sub>2</sub> binary modification and practically absent in the spectrum of Mn<sub>x</sub>O<sub>y</sub>-CeO<sub>2</sub> based composite. This confirms the XRD

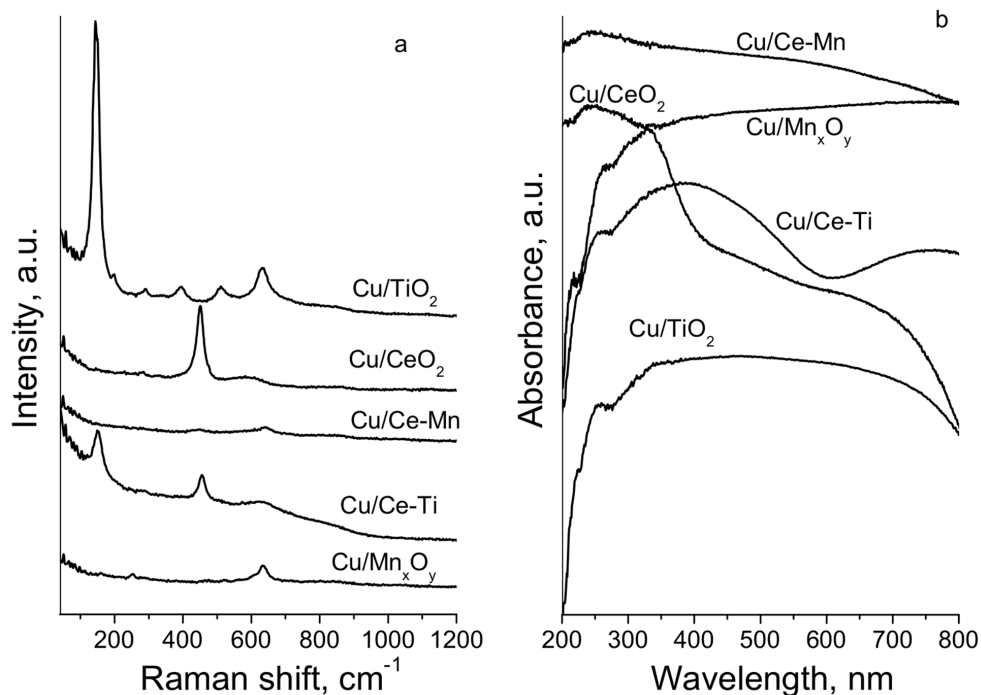


Fig. 2. Raman spectra (a) and UV-Vis (b) of the studied samples.

and Raman data for the formation of significantly large CuO particles in the former material and its exclusively high dispersion in the latter. Different interaction of the CuO species with highly defective binary oxides supports could be expected.

*Temperature-programmed reduction (TPR) with hydrogen*

The results from the TPR analyses are often complex for discussion due to the superposition of various effects, but the combination of this method with various physicochemical techniques is a promising approach for the elucidation of the oxidation state of metal ions and the variations in their environment (Fig. 3). Generally, the reduction of supported bulk CuO to Cu<sup>0</sup> is considered as one-step process, which maximum is in the range of 500–600 K, depending on the support used [19]. Nevertheless the nature of the support, the TPR–DTG curves for monocomponent supported modifications represent only one reduction peak, indicating uniformity of the loaded copper oxide species. In case of binary supported modifications, the reduction starts at lower temperature and the observed effect is complex in its shape. This indicates presence of different copper containing species. The low temperature effects could be assigned to copper species with higher dispersion and/or lower oxidative state which are in close contact with the defects of the binary oxide structure.

The high temperature effect belongs to relatively large CuO particles which weakly interact with the supports.

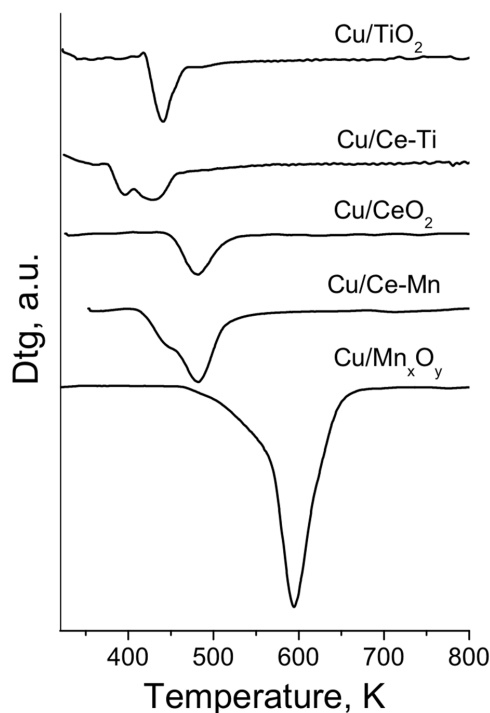
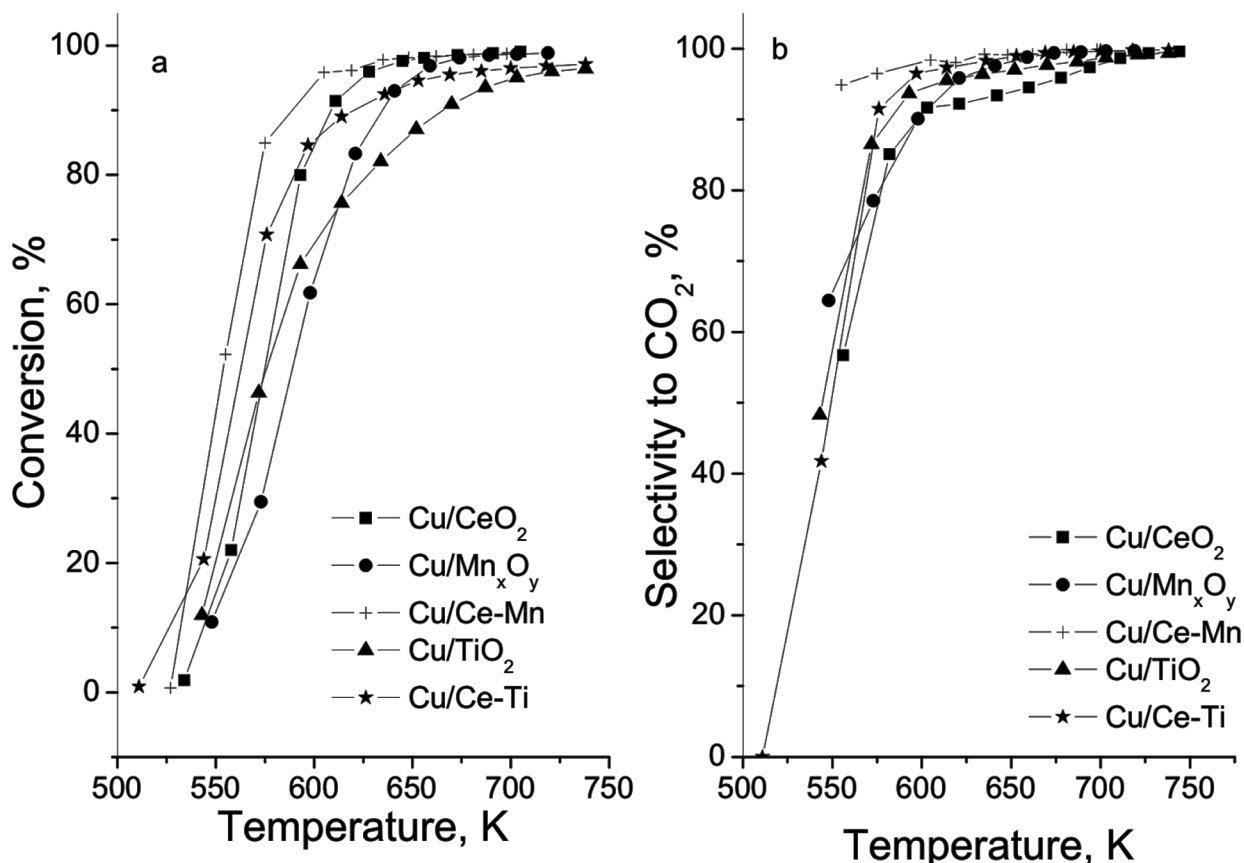


Fig. 3. TPR-DTG profiles of all modifications.



**Fig. 4.** Temperature dependency of ethyl acetate total oxidation (a) and selectivity to CO<sub>2</sub> (b) for the studied samples.

#### CATALYTIC TESTS

The catalytic properties of the samples were studied in temperature-programmed regime within the range of 423–773 K and the selectivity to the most important product from the oxidation reaction (CO<sub>2</sub>) is also presented (Fig. 4). From the obtained catalytic results it was clearly demonstrated that the synthesized oxide materials possess extremely high activity combined with enhanced selectivity to CO<sub>2</sub>. The ethyl acetate conversion is initiated at about 520 K and 80–100% conversion is achieved at 650 K. Generally, both binary supports show improved catalytic activity which could be assigned to the enhanced redox properties of the loaded copper species which is well demonstrated by the obtained TPR data (Fig. 3). The highest catalytic activity is registered for Cu/Ce-Mn sample and according to XRD, Raman, UV-Vis and TPR analyses this could be related to highest dispersion of CuO particles in contact with the significantly defective binary oxide structure. This seems to be favored by the better incorporation of Mn<sub>x</sub>O<sub>y</sub> into the CeO<sub>2</sub> lattice as compared to TiO<sub>2</sub>.

#### CONCLUSIONS

Multi-component materials on the base of copper, cerium, manganese and titanium oxides reveal good potential as catalysts for ethyl acetate elimination from VOCs emissions via total oxidation. The higher catalytic activity of binary oxides modifications is related to the stabilization of highly dispersed copper species in the vicinity of the support defects. As compared to TiO<sub>2</sub>, the improved solubility of Mn<sub>x</sub>O<sub>y</sub> in ceria and the variations in the manganese oxidative state provide the formation of more defective binary structure, which generates more finely dispersed and catalytically active copper oxide species.

**Acknowledgements:** Financial support from project DM-09/4/2016, Financial support by Program for career development of young scientists, BAS (project DFNP 17-65/26.07.2017) and Bulgarian Academy of Science – Czech Academy of Sciences bilateral project is gratefully acknowledged. The authors thank Dr. J. Henych for the nitrogen physorption and Raman investigation.

## REFERENCES

1. H. Kung, *Stud. Surf. Sci. Catal.*, **45**, 1 (1989).
2. Manoj B. Gawande, Rajesh K. Pandey, Radha V. Jayaram, *Catal. Sci. Technol.*, **2**, 1113 (2012).
3. Z. Ding, L. Li, D. Wade, E. Gloyna, *Ind. Eng. Chem. Res.*, **37**, 1707 (1998).
4. X. Tang, Y. Li, X. Huang, Y. Xu, H. Zhu, J. Wang, W. Shen, *Appl. Catal. B: Environ.*, **62**, 265 (2006).
5. L. Shi, W. Chu, F. Qu, S. Luo, *Catal. Lett.*, **113**, 59 (2007).
6. R. Ivanova, T. Tsoncheva, *Bulg. Chem. Commun.*, **49**, 176 (2017).
7. S. Limin, C. Wei, Q. Fenfen, H. Jinyan, L. Minmin, *J. Rare Earths*, **26**, 836 (2008).
8. M. Gawande, R. Pandey, R. Jayaram, *Catal. Sci. Technol.*, **2**, 1113 (2012).
9. X. Yao, Q. Yu, Z. Ji, Yuanyuan Lv, Y. Cao, C. Tang, F. Gao, L. Donga, Y. Chen, *Appl. Catal. B: Environ.*, **130–131**, 293 (2013).
10. X. Chen, S. Carabineiro, S. Bastosa, P. Tavares, J. Órfão, M. Pereira, J. Figueiredo, *Appl. Catal. A: Gen.*, **472**, 101 (2014).
11. J. Liu, X. Li, Q. Zhao, D. Zhang, P. Ndokoy, *J. Mol. Catal. A: Chem.*, **378**, 115 (2013).
12. X. Yoo, L. Zhanga, L. Li, L. Liua, Y. Caoa, X. Dong, F. Gao, Y. Deng, C. Tang, Z. Chen, L. Donga, Y. Chena, *Appl. Catal. B: Environ.*, **150–151**, 315 (2014).
13. T. Tsoncheva, G. Issa, T. Blasco, M. Dimitrov, M. Popova, S. Hernández, D. Kovacheva, G. Atanasova, J.M. López Nieto, *Appl. Catal. A: General*, **453**, 1 (2013).
14. H. Hagemann, H. Bill, W. Sadowski, E. Walker, M. Francois, *Solid State Commun.*, **73**, 447 (1990).
15. M. Dimitrov, R. Ivanova, N. Velinov, J. Henych, M. Slušná, V. Štengl, I. Mitov, T. Tsoncheva, J. Tolasz, *Nano-Struct. & Nano-Objects.*, **7**, 56 (2016).
16. A. Kambolis, H. Matralis, A. Trovarelli, Ch. Papadopoulou, *Appl. Catal., A: Gen.*, **377**, 16 (2010).
17. Y. Lin, S. Ming, Y. Jian, Y. Qian, H. Zhifeng, L. Chaosheng, *Chin. J. Catal.*, **29**, 1127 (2008).
18. T. Tsoncheva, D. Kovacheva, J. Henych, V. Štengl, R. Ivanova, *Reac. Kinet. Mech. Cat.*, **116**, 397 (2015).
19. P. Ratnasamy, D. Srinivas, C. Satyanarayana, P. Manikandan, R. Senthil Kumaran, M. Sachin, V. Shetti, *J. Catal.*, **221**, 455 (2004).